Experimental study of the impact of geometrical defects on the high cycle fatigue behavior of polycrystalline aluminium with different grain sizes

Benoît Bracquart[a,*], Charles Mareau[a], Nicolas Saintier[b], Franck Morel[a]

[a] *Arts et Métiers ParisTech, Campus d'Angers, LAMPA, 2 bd du Ronceray, 49035 Angers Cedex 1, France*
[b] *Arts et Métiers ParisTech, Campus de Bordeaux-Talence, I2M, Esplanade des Arts et Métiers, 33405 Talence, France*

Abstract

Geometrical defects are known to have a detrimental influence on the high cycle fatigue resistance of metallic alloys, smaller defects being less harmful. In this experimental work, the influence of the defect size on the high cycle fatigue behavior of polycrystalline aluminium with different grain sizes is investigated, to better understand the role of internal length scales. Firstly, different thermomechanical treatments are applied to obtain aluminium samples with either small (100 µm) or large (1000 µm) grains. The samples are used for preparing fatigue specimens, with either small (100 µm) or large (1000 µm) hemispherical defects. Fully reversed stress-controlled fatigue tests are then carried out. According to fatigue test results, surface crack initiation is delayed when the grain size is reduced, while an approximation of the fatigue limit shows that it is not much influenced by the average grain size. The influence of grain size seems to be explained by the role of cyclic plasticity in the crack initiation process. Finally, Electron BackScattered Diffraction (EBSD) maps are collected for specimens with large grains and small defects. Based on this experimental dataset, fatigue crack initiation from a defect is found to be strongly impacted by the

*Corresponding author
URL: benoit.bracquart@ensam.eu (Benoît Bracquart)

crystallographic orientation of the surrounding grain, crack initiation preferably occurring in crystals being favorably oriented for plastic slip.

Keywords: aluminium, grain size, defects, high cycle fatigue, crack nucleation

1. Introduction

In metallic alloys, defects can originate from material elaboration [1], manufacturing processes [2, 3] or foreign-object impacts [4]. These defects have either a geometrical (*e.g.* notches) or metallurgical (*e.g.* inclusions) nature and can be of various shapes and sizes. Because they act as stress concentrators, such defects usually have a detrimental influence on the high cycle fatigue (HCF) resistance of metallic alloys [5]. The fatigue resistance reduction associated with the presence of defects is however strongly dependent on their size; the reduction being higher for a larger defect. Endo *et al.* [6] and Luk´as *et al.* [7] also showed that there exists a critical defect size below which the fatigue behavior is no longer affected. Although the knowledge of the critical size is important to design fatigue-resistant structures, the dependence of this critical size regarding microstructural features remains unclear.

Important experimental efforts have been made to characterize the role of microstructural features on the fatigue behavior in the absence of significant geometrical defects. For instance, the influence of grain size on the fatigue behavior of smooth specimens is largely documented [8, 9, 10]. The fatigue limit is usually found to increase when the grain size is reduced and the influence of grain size on the fatigue limit is often correctly described with an Hall-Petch [11, 12] type of relation ($\sigma_D = \sigma_0 + k/\sqrt{\phi}$, where σ_D is the fatigue limit, ϕ the mean grain size, and σ_0 and k are material constants) [13]. According to Chan [14], the influence of grain size is explained by the fact that polycrystals with large grains are more prone to initiate cracks in slip bands than their smaller- grained counterparts, leading to earlier crack initiation in the former. The

influence of grain size on fatigue crack propagation in aluminium polycrystals has been investigated by Saga *et al.* [15, 16]. They conclude that the larger the grains, the higher the crack growth rate and the lower the number of cycles to failure. Thompson *et al.* [17] concluded differently regarding the influence of grain size on the fatigue behavior of aluminium polycrystals. Indeed, with an average grain size in the range 20–200 µm, no significant impact on the fatigue resistance at 10^6 cycles has been observed. Their interpretation is that cross-slip can easily be activated in pure aluminium, and that the resulting cellular dislocation structures tend to hide grain boundaries in the crack propagation stage.

Very few attempts have been made to investigate the impact of microstructure on the fatigue behavior of metallic specimens with geometrical defects. Guerchais *et al.* [18] studied the influence of local microstructure around the notch for different loading conditions, but only the defect size and local microstructure were varied, not the grain size. Sweeney *et al.* [19] and Wan *et al.* [20] relied on a comprehensive experimental procedure, including HCF tests and systematic Electron BackScattered Diffraction (EBSD) maps, to set up numerical models in order to predict fatigue crack initiation. They propose a stored energy based criterion to predict the crack initiation location and the number of cycles necessary to initiate a crack. In their case, the microstructure is varied around the defect, but grain and defect sizes are held constant. To explore the connection between grain size and defect size, Karry *et al.* [21] carried out an experimental investigation on brass specimens with defects of different sizes and shapes, as well as on smooth specimens. They observed that when a defect is introduced, the decrease in fatigue limit compared to the corresponding smooth specimen was lower for a higher grain size. The defect sensitivity is thus higher for small grained microstructures. Lorenzino *et al.* [22] carried out fatigue tests on pure

aluminium specimens with different grain and defect sizes. Besides the fact that a larger grain size and/or notch size reduces the fatigue limit, they showed that, as far as crack propagation is concerned, the governing parameter is the relative defect size (the defect size divided by the mean grain size) rather than the absolute physical one. Indeed, by normalizing the fatigue limit of specimens with defects by the fatigue limit of smooth specimens with the same grain size, and the defect size by the grain size, all data points fall onto the same line in a fatigue limit/notch size diagram. Vincent *et al.* [23], using various defect sizes and grain sizes, came to the same conclusion for commercially pure iron. Those two studies focus on the number of cycles to failure rather than to crack initiation, but they demonstrate the interest of varying both characteristic sizes.

In the present work, an experimental campaign is carried out to investigate the joint influence of geometrical surface defect size and grain size on the HCF behavior of pure aluminium polycrystals. In contrast with the work of Lorenzino *et al.* [22], who focused on crack propagation, this study concentrates on crack initiation in the presence of defects. Indeed, the influence of the defect is most important in the crack initiation stage, as it acts as a stress concentrator and a preferential crack initiation site; its influence becomes lower once a crack is initiated and starts to propagate. Also, to better understand the factors governing the initiation of a fatigue crack, Electron Backscattered Diffraction (EBSD) techniques are used to evaluate the influence of crystallographic orientation.

The present paper is organized as follows. Firstly, the experimental procedure used for preparing aluminium specimens and performing fatigue tests is detailed. Then, the experimental results, which have been obtained for reversed uniaxial tension-compression loading conditions, are presented. The results are finally discussed to establish a connection between plasticity and crack initiation.

2. Experimental procedure

2.1. Material description

The material used in this study is a commercial purity aluminium (AA1050), for which the aluminium weight concentration exceeds 99.5%. The alloy is supplied in the form of 6 mm-thick cold-rolled sheets. The initial microstructure is composed of elongated grains along the rolling direction.

Two different thermomechanical sequences have been applied to control the grain size ϕ, which is evaluated by the average grain intercept method. For the first sequence, in addition to the strain-hardening associated to the rolling process, aluminium samples are held at 550°C for 45 minutes and then air cooled. The resulting microstructure is referred to as "small" grain microstructure (denoted by subscript s) with an average grain size ϕ_s of about 100 µm along the rolling direction. For the second sequence, samples are firstly maintained at

550°C for 2 hours and then air-cooled. A tensile strain of 12% is then applied at room temperature in the rolling direction, followed by a second heat treat ment at 600°C for 2 hours, before a final air cooling. The corresponding grain size ϕ_l is approximately of 1000 µm along the rolling direction. This second microstructure is referred to as "large" grain microstructure (denoted by sub-script l). Figure 1 illustrates optical micrographs of the initial, large grain and small grain microstructures, in a section parallel to the rolling direction. Both sequences ending with a recrystallization treatment, they provide fully annealed microstructures with different grain sizes.

Grain sizes have been evaluated in the three principal sheet directions from several micrographs. For both microstructures, grain sizes along the rolling and transverse directions are identical. The average grain size is however smaller, by a factor of 2, along the normal direction. It should be noticed that, for a given microstructure, all samples have been extracted from the same aluminium

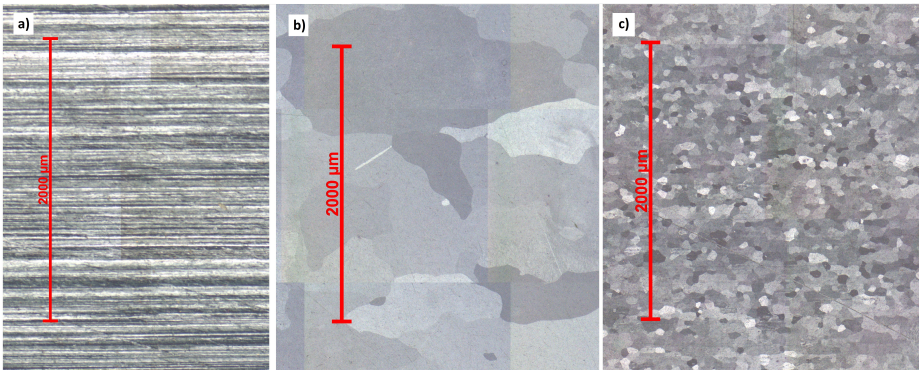

Figure 1: Optical micrographs of the a) initial, b) large grain and c) small grain microstructures. The normal direction is vertical.

sheet. Also, during the preparation stage, some samples have been randomly selected to check the repeatability of the preparation procedure.

Tensile tests have been performed on both microstructures, in the rolling direction, using a strain rate $\dot{\varepsilon} = 10^{-3}s^{-1}$. The corresponding mechanical properties are presented in Table 1. One can note that the values of $R_{p0.2}$ and R_m are lower for a higher grain size, in accordance with the classical Hall-Petch law.

	$R_{p0.2}$ (MPa)	R_m (MPa)	$A(\%)$
$\phi_s = 100\ \mu m$	17.8	61.7	50.3
$\phi_l = 1000\ \mu m$	16.1	60.7	48.1

Table 1: Tensile mechanical properties of polycrystalline aluminium for both grain sizes. Tensile tests have been performed with a strain rate $\dot{\varepsilon} = 10^{-3}s^{-1}$.

2.2. Specimen preparation

Fatigue specimens have been machined from previously prepared aluminium samples. The geometry of fatigue specimens is presented in Figure 2. The gauge section is 15 mm-long and 30 mm-wide, the thickness is 5 mm and the loading axis coincides with the rolling direction. For the large grain microstructure, particular care has been taken to extract the gauge part of fatigue specimens from the area where the applied tensile strain, hence the grain size, had been

controlled.

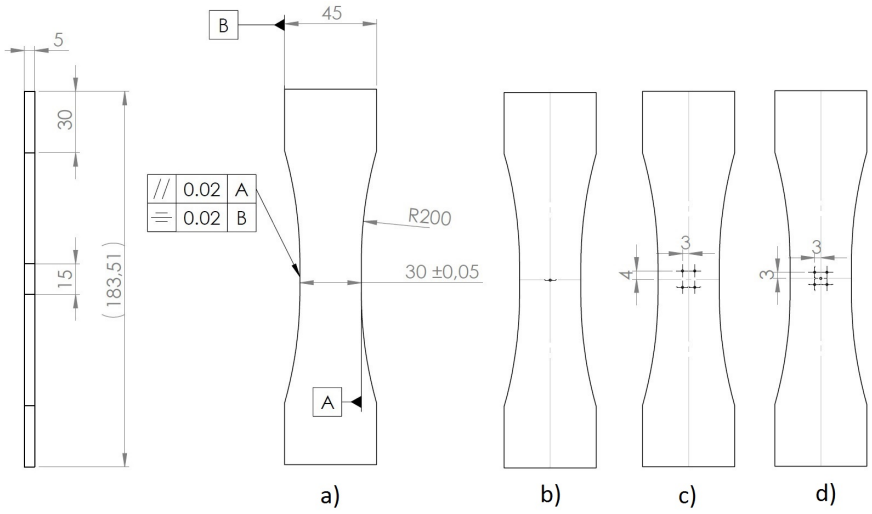

Figure 2: Geometry of fatigue specimens. a) smooth, b) single large defect (SLD), c) multiple large defects (MLD) and d) multiple small defects (MSD) specimens.

Geometrical defects have been introduced in the gauge area of fatigue specimens with a hemispherical drill, the defect size d being thus given by the drill diameter. A high cutting speed and a low translation speed (1 µm.s^{-1}) have been used to ensure that the local microstructure is not affected by drilling operations. In the present work, two defect sizes have been considered: $d_s = 100$ µm and $d_l = 1000$ µm, where subscripts s and l denote respectively the small and the large defects. Defect depths and shapes have been systematically inspected with a 3D profilometer. For small defects, the relative difference between the nominal depth and the actual depth is under 5% in most cases, and under 10% in all cases. For large defects, this difference is always inferior to 1%.

Four different types of specimens are used: smooth specimens, specimens with a single large defect (denoted SLD specimens), specimens with multiple large defects (MLD specimens) and specimens with multiple small defects (MSD specimens). Respectively 4 and 5 defects are machined in one specimen, for

MLD and MSD specimens. Figure 2 displays the location(s) of defect(s) relative to the center of the gauge section.

Fatigue specimens are then submitted to mechanical polishing (FEPA abrasives 600, 1200 and 2000), followed by a final heat treatment (260°C for 2 hours and air-cooling) to relieve the residual stresses resulting from machining and polishing operations. The temperature for this heat treatment is chosen low enough not to engage recrystallization and modify the grain size.

2.3. Experimental set-up

Fully reversed load-controlled push-pull fatigue tests (*i.e.* $R_\sigma = -1$) are carried out on an Instron 8802 servohydraulic testing machine. The tests are thus nominal-stress-controlled; for the sake of simplicity, they are referred to as "stress-controlled" in the following. Different tests frequencies, namely 1 Hz and 12 Hz, are used, depending on the kind of test performed. To prevent buckling of the specimen while allowing elongation measurement by an extensometer, a specific anti-buckling fixture has been developed. As shown in Figure 3, it consists of two opposing asymmetrical steel plates which are assembled to exert a normal effort on the specimen during the compression stage. A teflon film is placed between the specimen and the fixture to reduce friction.

Preliminary tests have been conducted on a specimen equipped with strain gauges to verify that, despite the additional effort due to the fixture, the stress state in the center of the gauge area is not altered. However, when no defect is introduced, cracks initiate and propagate from the interface between the specimen and the rectangular plate in a region where the stress field might be perturbed. As a result, smooth specimens cannot be used to characterize the fatigue behavior since the stress state might not be correctly controlled in the crack initiation area. Smooth specimens are thus solely used for the evaluation of the cyclic behavior.

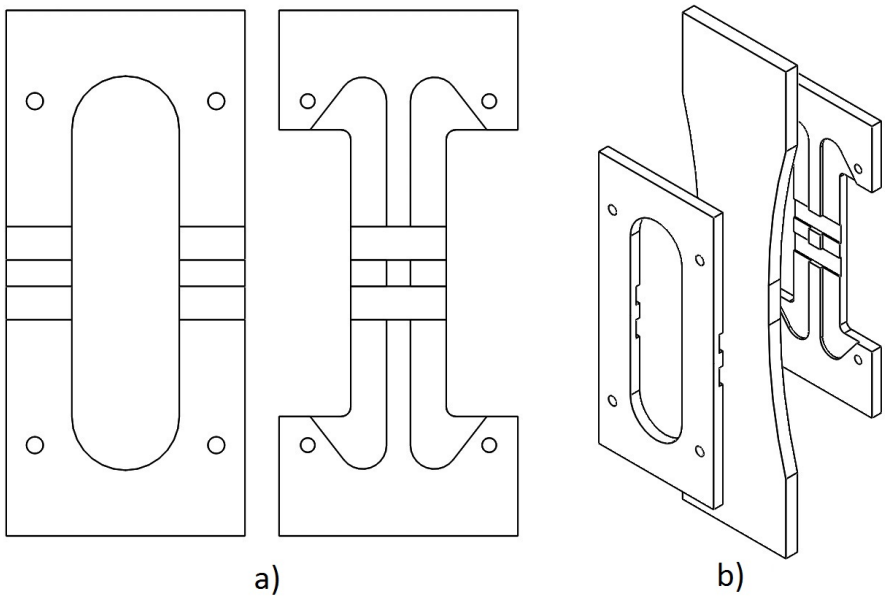

Figure 3: a) Geometries of the two opposing plates of the anti-buckling fixture, and b) exploded view of the assembly on fatigue specimen.

For specimens with defects, the final failure of fatigue specimens does not always result from a defect-induced crack. As a consequence, when evaluating the influence of geometrical defects on the number of cycles to failure, only tests for which fatigue failure is caused by defects have been considered. This aspect is not problematic for large defects ($d_l = 1000$ µm), as final failure is caused by defects in most cases. However, for small defects ($d_s = 100$ µm), final failure often results from another crack than the one(s) initiated from the defect. As a consequence of the propagation of non defect-induced cracks, the stress field in the vicinity of defects can be strongly perturbed. Therefore, for small defects, only crack initiation, for which perturbations caused by cracks initiated away from defects are negligible, is investigated.

Different experimental configurations are used to investigate the influence of grain size and/or defect size. In the first one, the cyclic elastic-plastic behavior of pure aluminium is evaluated from smooth specimens of both grain sizes

equipped with a clip-on Instron extensometer with a 12.5 mm spacing. The second configuration uses SLD specimens (d_l = 1000 µm). This configuration aims at measuring the length of cracks having been initiated from the defect. For this application, the area surrounding the defect is observed with an optical camera and pictures are recorded every 1000 loading cycles. While an *in-situ* monitoring of the crack length is possible with this second configuration, the detection is limited to surface cracks with a minimum length of about 100 µm. Due to the potential influence of non defect-induced cracks, small defects are not studied in this configuration. The third configuration uses MLD and MSD specimens (d_l = 1000 µm and d_s = 100 µm). For a given low stress amplitude, preventing macroscopic crack propagation, it allows determining the number of cracked defects from *a posteriori* Scanning Electron Microscopy (SEM) observations. Some of the MSD specimens are also selected to carry out EBSD observations of the microstructure surrounding the defect.

3. Results

3.1. Smooth specimens

As discussed earlier, smooth specimens have been used to investigate the influence of grain size on the cyclic elastic-plastic behavior of pure aluminium. Fully reversed stress-controlled cyclic tests have been performed with a loading frequency of 1 Hz and a constant stress amplitude σ_a, for both grain sizes (ϕ_s and ϕ_l). Most tests have been stopped after 10^4 cycles, but some have been continued up to 10^5 or 2 $\times$ 10^5 cycles to determine whether elastic shakedown is observed or not. The evolution of the axial plastic strain range $\Delta\varepsilon^p$ as a function of the number of cycles N is plotted for different stress amplitudes in Figures 4 and 5, respectively for small and large grains.

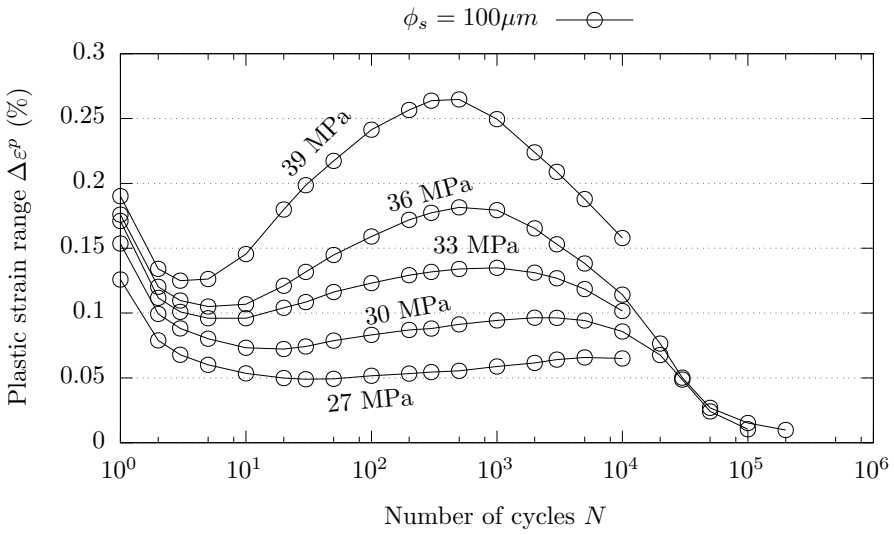

Figure 4: Evolution of $\Delta\epsilon^p$ during cycling for ϕ_s, for different stress amplitudes.

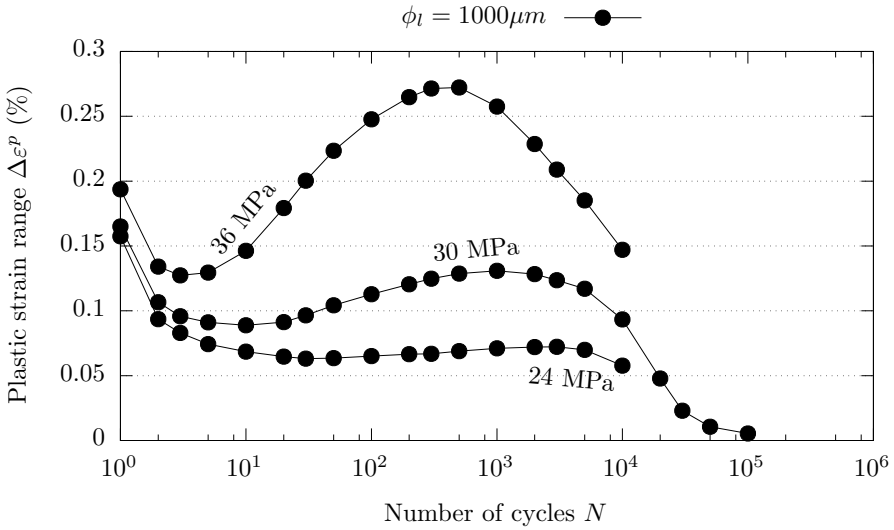

Figure 5: Evolution of $\Delta\epsilon^p$ during cycling for ϕ_l, for different stress amplitudes.

3.2. Specimens with a single large defect (SLD)

Stress-controlled fatigue tests have been carried out on SLD specimens (d_l = 1000 µm) to evaluate the impact of grain size on fatigue crack initiation and

specimen fracture. For these tests, the loading frequency is set to 12 Hz. In the absence of failure, fatigue tests have been interrupted after 10^6 cycles. The observation of the area surrounding the defect with the optical camera allows monitoring early crack propagation from the defect, on the specimen surface, as illustrated in Figure 6 for the ($d_l - \phi_s$, σ_a=30 MPa) configuration, for which failure occurred at 292,000 cycles.

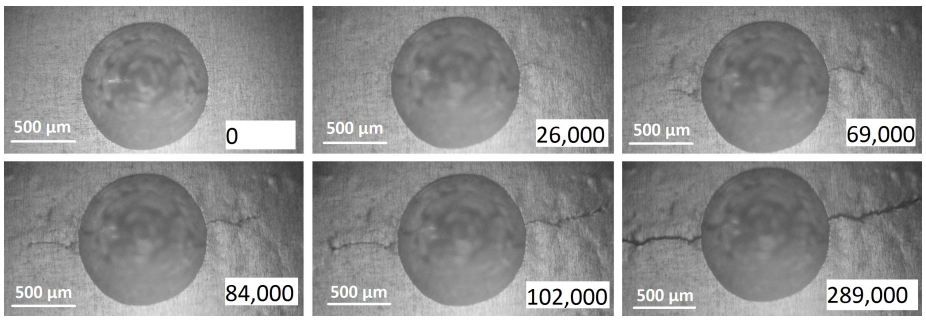

Figure 6: Example of crack monitoring during fatigue test of a SLD specimen. The number of cycles is indicated in the bottom right corner of each picture. Loading axis is vertical.

Based on fatigue test results, two different S-N diagrams have been plotted. The first S-N diagram, Figure 7, represents the evolution of the stress amplitude

σ_a as a function of the number of cycles to failure N_f, the failure being defined as the separation of the specimen into two distinct parts. Note that for large grains (ϕ_l = 1000 µm), for respectively $\sigma_a = 30$ MPa and $\sigma_a = 33$ MPa, only 2 and 1 point(s) were representative (failure from the crack initiating from the defect). The evolution of the stress amplitude as a function of the number of cycles to crack initiation N_i is displayed in a second S-N diagram, Figure 8. In the present work, the crack initiation criterion, defining N_i, is arbitrarily set to a total surface crack length of 100 µm, which is the shortest detectable crack length. One should note that, as a result, especially for the small grain microstructure, the number of cycles to crack initiation may include a portion of early crack propagation.

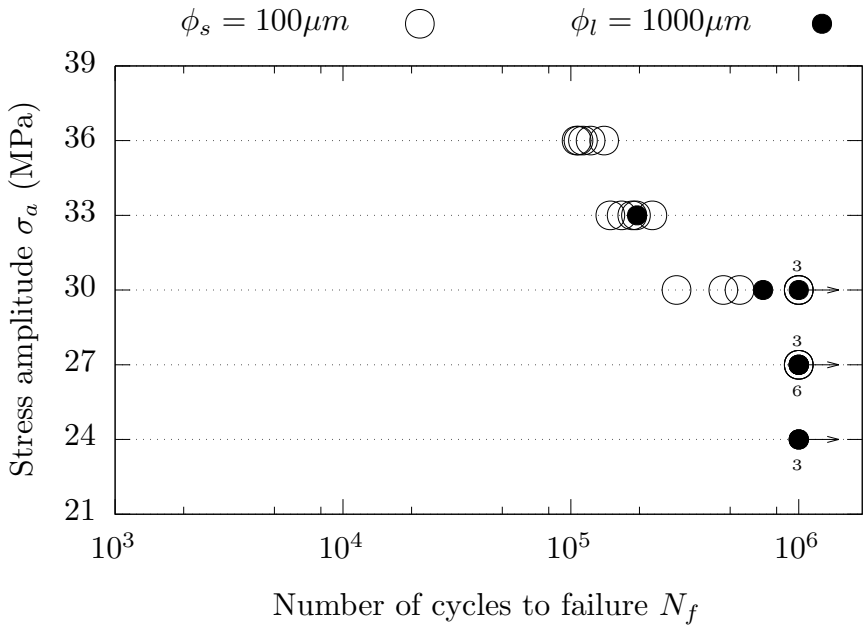

Figure 7: S-N curves for failure, obtained for SLD specimens (d_l =1000 µm) and two sizes of microstructure. Arrows represents run-out specimens. Numbers indicates the superimposed points (above for ϕ_s, below for ϕ_l).

3.3. Specimens with multiple defects (MLD and MSD)

To investigate the influence of defect size on fatigue crack initiation, some specimens with multiple defects have been submitted to stress-controlled fatigue tests. The fatigue tests are conducted with a frequency of 12 Hz and up to 10^6 loading cycles. In this case, both the grain size ϕ and the defect size d are varied. Stress amplitudes are selected low enough to prevent macroscopic crack propagation (hence failure) and exclude interactions between defects.

After fatigue testing, SEM observations of each defect are carried out to determine whether a crack initiated or not. In comparison with the *in-situ* monitoring used earlier, short cracks are more accurately detected with SEM because it allows observing the bottom pole of hemispherical defects. Crack initiation can thus be detected more precisely with this method. The results

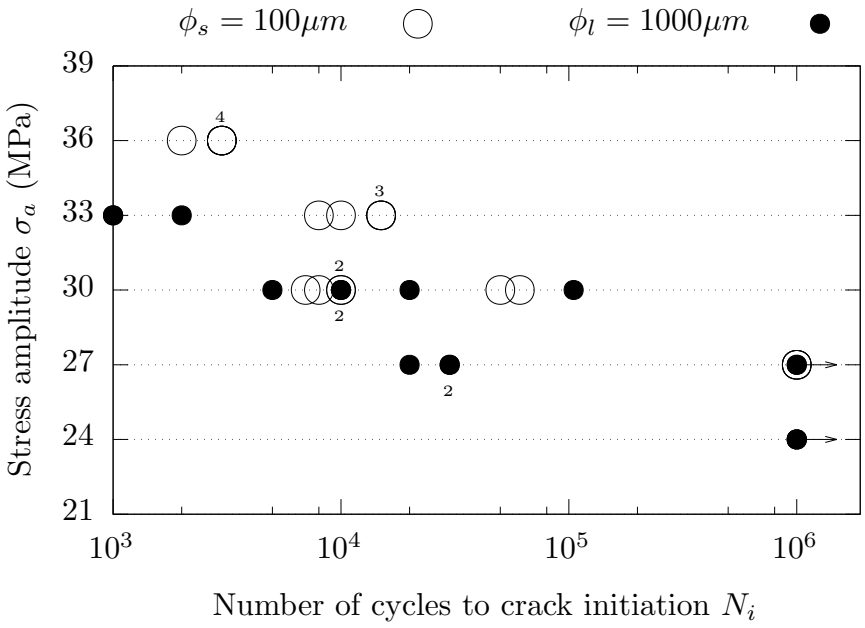

Figure 8: S-N curves for crack initiation, obtained for SLD specimens (d_l =1000 µm) and two sizes of microstructure. Crack initiation criterion: 100 µm-long surface crack. Arrows represents run-out specimens for which this criterion was not reached. Numbers indicates the superimposed points (above for ϕ_s, below for ϕ_l).

obtained for different grain sizes, defect sizes and stress amplitudes are presented in Table 2, which shows the proportion of cracked defects in the different configurations.

	$d_s = 100\ \mu m$		$d_l = 1000\ \mu m$	
	σ_a (MPa)	n_c/n	σ_a (MPa)	n_c/n
$\phi_s = 100\ \mu m$	27	1/15	24	0/8
	28.5	8/15	27	10/12
	30	11/15	28.5	11/11
$\phi_l = 1000\ \mu m$	24	1/15	24	0/17
	25.5	4/15	25.5	7/16
	27	9/15	27*	7/8

Table 2: Proportion of cracked defects for the four $d - \phi$ configurations (MLD and MSD specimens), for different stress amplitudes σ_a. n is the total number of defects studied in the configuration and n_c the number of cracked defects after cycling (* denotes a high stress level leading to a macroscopic crack propagation and possibly failure of the specimen).

Based on these results, the stress amplitude corresponding to a 50% probability of crack initiation to a defect, $\sigma_a(P_{50})$, has been estimated for each $d-\phi$ configuration, by linear interpolation (see Figure 9).

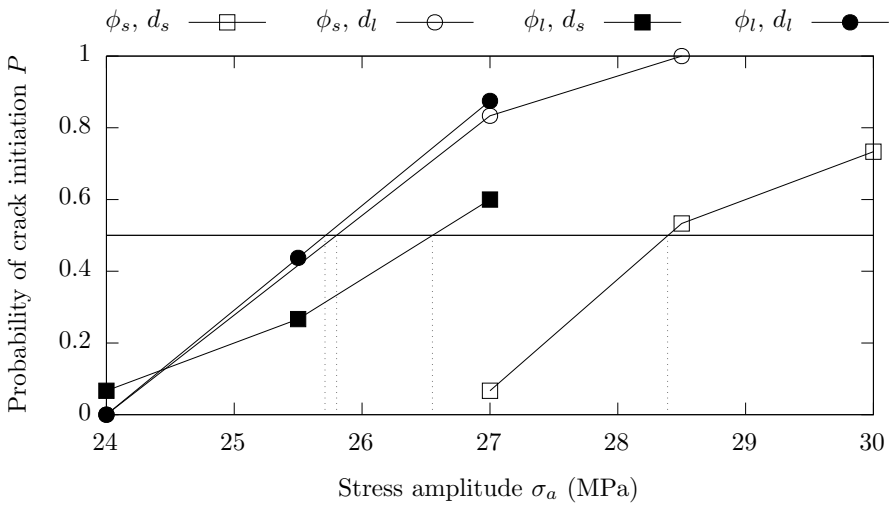

Figure 9: Probability P of crack initiation to the defect, for the different $d-\phi$ configurations (MLD and MSD specimens), as a function of the applied stress amplitude σ_a.

4. Discussion

4.1. Influence of grain size and defect size

Based on the experimental results, the influence of grain size and/or defect size on the HCF behavior of pure aluminium is firstly discussed.

According to Figures 4 and 5, for both the small and large grain microstructures, the cyclic behavior is composed of three successive stages: primary hardening, softening and secondary hardening. This specific behavior, which is explained by the formation and evolution of dislocation structures [24, 25, 26, 27], has already been highlighted by Giese *et al.* [28] and Videm *et al.* [29]. In the following, the plastic strain range, determined at the transition between

the softening and secondary hardening stages, is arbitrarily chosen as a macroscopic plastic activity indicator for given grain size and stress amplitude. This quantity, denoted by $\Delta\varepsilon^p_{s-h}$, is plotted as a function of the stress amplitude in Figure 10.

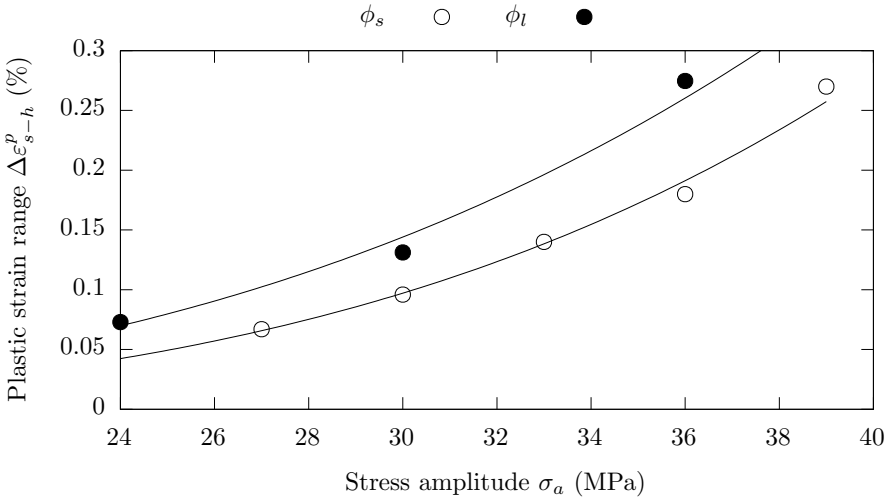

Figure 10: Evolution of $\Delta\varepsilon^p_{s-h}$ as a function of the stress amplitude σ_a, for both microstructures.

Figure 11 shows, for all SLD specimens that failed from the defect before 10^6 cycles, the ratio between the crack initiation life and the total fatigue life. Most of the fatigue life is spent in the propagation stage, the ratio N_i/N_f being under 0.1 in all cases. Since, as shown in Figure 7, the fatigue limit (estimated as the higher stress level for which no failure occurs) is not much influenced by grain size, this gives credit to the interpretation of Thompson *et al.* [17], *i.e.* intragranular dislocation structures can hide grain boundaries in the crack propagation stage. On the contrary, the crack initiation stage may be impacted by the average grain size. Indeed, as illustrated by Figure 8, the mean number of cycles to crack initiation N_i is reduced when the grain size is increased. However, this last conclusion must be taken with caution, as it depends on the

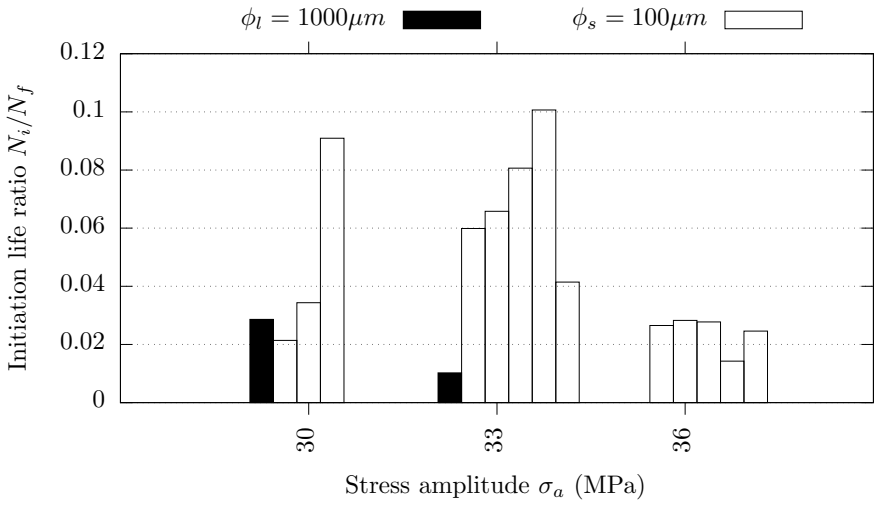

Figure 11: Ratio between the number of cycles to surface crack initiation N_i and the number of cycles to failure N_f, as a function of the stress amplitude σ_a, for all SLD specimens that failed from the defect before 10^6 cycles.

crack initiation criterion used. Indeed, as can be seen in Figure 9, there are no differences in the stress amplitudes necessary to initiate a crack from a large defect, between the two grain sizes. The different conclusions can be explained by the fact that a small portion of early crack propagation is necessary to reach the crack initiation criterion (100-µm long surface crack) in the results of Figure 8, whereas the criterion used in the results of Figure 9 is more precise.

	$d_s = 100\ \mu m$		$d_l = 1000\ \mu m$	
	$\sigma_a(P50)$ (MPa)	$\Delta\varepsilon^p_{s-h}(P50)(\%)$	$\sigma_a(P50)$ (MPa)	$\Delta\varepsilon^p_{s-h}(P50)(\%)$
$\phi_s = 100\ \mu m$	28.4	0.079%	25.8	0.056%
$\phi_l = 1000\ \mu m$	26.6	0.098%	25.7	0.087%

Table 3: For each of the four $d - \phi$ configurations (MLD and MSD specimens): macroscopic stress amplitude for 50% probability of crack initiation at the defect, $\sigma_a(P50)$, and corresponding macroscopic plasticity level, $\Delta\varepsilon^p_{s-h}(P50)$ (determined at $\sigma_a(P50)$ for the corresponding smooth specimen).

This influence of grain size on fatigue crack initiation is also observed for specimens with multiple defects. Indeed, as shown in Table 3, the stress am-

plitude corresponding to a 50% crack initiation probability, $\sigma_a(P50)$, is lower for the large grain microstructure, when small defects are introduced (reduction of 1.8 MPa, *i.e.* 6.3%, between both grain sizes). For large defects, however, the difference between both grain sizes is negligible (this difference with the *in-situ* crack monitoring approach on SLD specimens presented above being attributable to the different crack initiation criteria used, as discussed earlier). The small grain microstructure is thus more sensitive to defect size. This difference regarding defect size sensitivity can be interpreted in terms of plastic

activity. Table 3 illustrates the change in plastic activity, given by $\Delta\varepsilon^p_{s-h}$, between the four $d-\phi$ configurations. Values have been obtained by coupling the stress levels of Table 3 and the results of Figure 10. When increasing the defect size, the change in plastic activity is more significant for the small grain microstructure (relative reductions of 29% and 11%, from a small to a large defect, respectively for the small grain and the large grain microstructures).

Figure 12 shows that, for a constant relative defect size d/ϕ but different absolute sizes, the plastic activity corresponding to a 50% crack initiation probability is about the same for both grain sizes (less than 10% relative variation). This is consistent with the results of Lorenzino *et al.* [22] and Vincent *et al.* [23] who observed that the relative defect size d/ϕ is more relevant than the actual physical defect size d. The equivalence of plasticity levels for a given ratio suggests that, on a macroscopic point of view, regardless of the local microstructural features (e.g. crystallographic orientation, grain shape) which can influence variability of crack initiation behavior for a given $d-\phi-\sigma_a$ configuration, crack initiation is essentially governed by plasticity.

4.2. Influence of local microstructure

To better understand the role of microstructure on fatigue crack initiation, EBSD analyses have been carried out on specimens which have been submitted

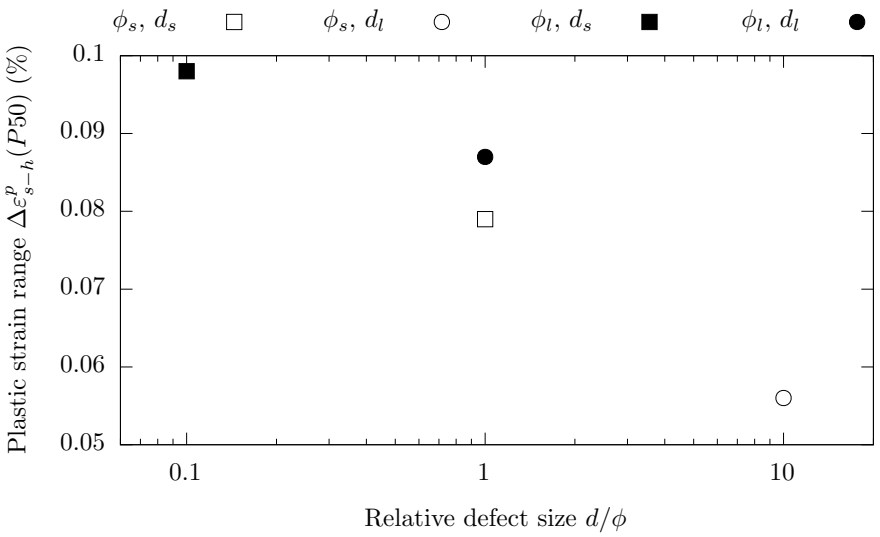

Figure 12: Plastic indicator for a probability of crack initiation to a defect of 50%, $\Delta\varepsilon^p_{s-h}(P50)$, as a function of the relative defect size d/ϕ, for the four $d-\phi$ configurations (MLD and MSD specimens).

to a reversed stress-controlled fatigue test up to 10^6 cycles. The analyses have been performed *a posteriori* on MSD specimens with large grains ($d_s - \phi_l$). In this specific configuration, defects are usually embedded within a single grain (see examples of cleaned EBSD maps, Figure 13). It is therefore possible to associate a unique crystallographic orientation to each defect (among the 33 defects studied, only one lies on a grain boundary, and was therefore excluded from the analysis). The same stress amplitude ($\sigma_a = 27$ MPa) has been used for all observed specimens.

To evaluate the influence of crystallographic orientation on fatigue crack initiation, the maximum Schmid factor has been determined for each defect. The maximum Schmid factor corresponds to the ratio between the shear stress acting on the primary slip system and the applied uniaxial stress. Grain orientations of cracked and uncracked defects are plotted in Figure 14 in the stereographic unit triangle. Crack initiation is found to be highly dependent on crystallographic

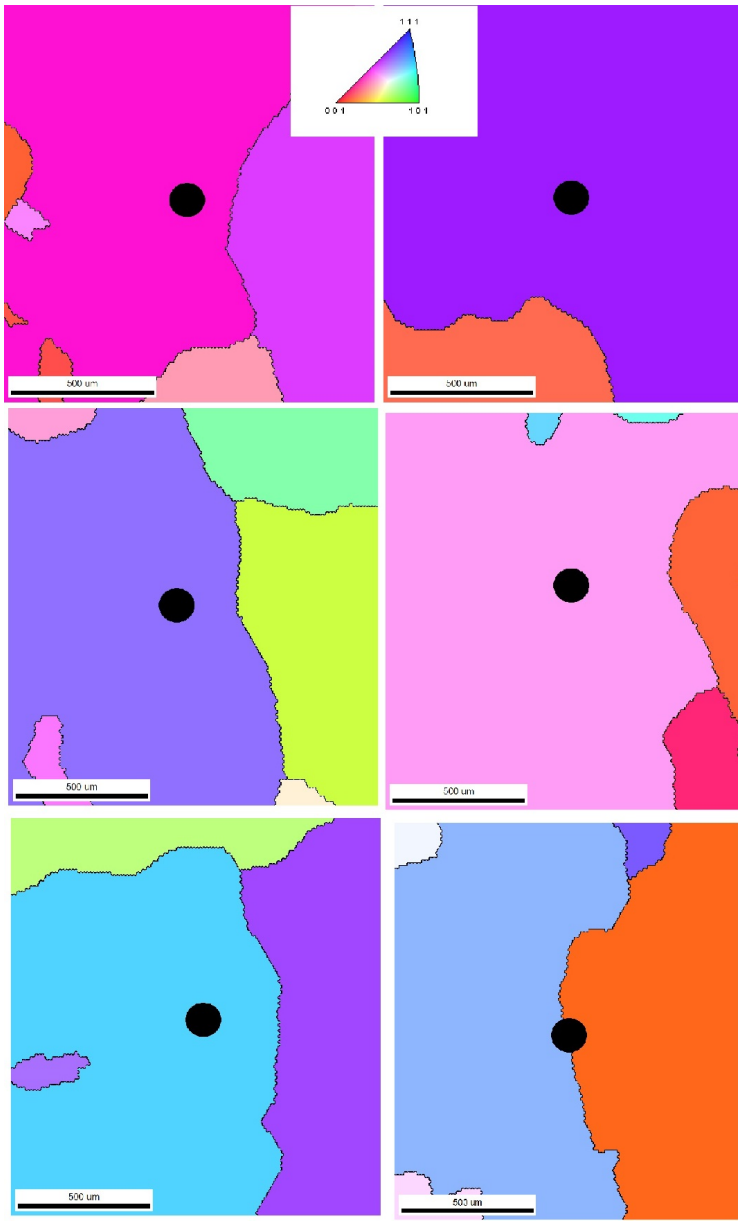

Figure 13: Examples of cleaned EBSD maps on MSD specimens. The defect is represented by the black disk. Bottom right map shows the configuration where the defect lies on a grain boundary (excluded from the analysis).

orientation, as grains being favorably oriented for plastic slip are more prone to crack initiation.

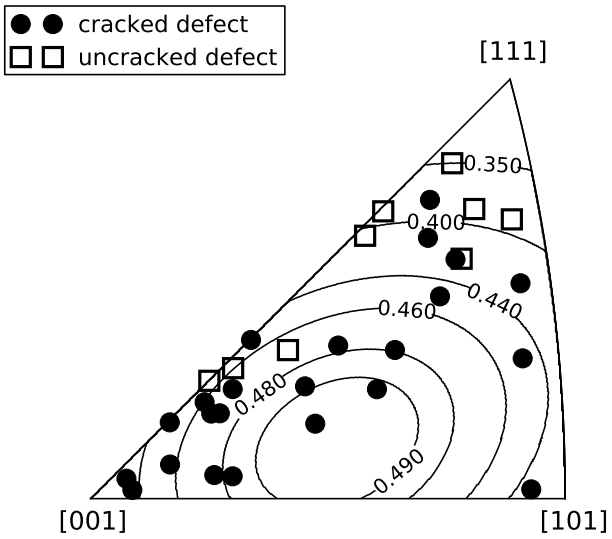

Figure 14: Orientation of the grains embedding defects, regarding the loading axis, with values of the Schmid factor on the primary slip system.

To evaluate the possible influence of normal stresses, the ratio between the maximum normal stress acting on the slip systems and the applied uniaxial stress has been determined for each defect, with a similar approach. The results are presented in Figure 15. One can note that normal stresses have no obvious influence on fatigue crack initiation.

A posteriori SEM observations of cracked defects often do not allow for a clear identification of the crack initiation plane. However, for one cracked defect, this plane can be identified. From EBSD data, the maximum Schmid factor has been calculated for each of the four {111} slip planes of the surrounding grain. Figure 16 shows this cracked defect, the slip planes traces (i.e. the directions of the intersections of slip planes with a surface parallel to the free surface, as is approximately the defect root), and the corresponding values of maximum

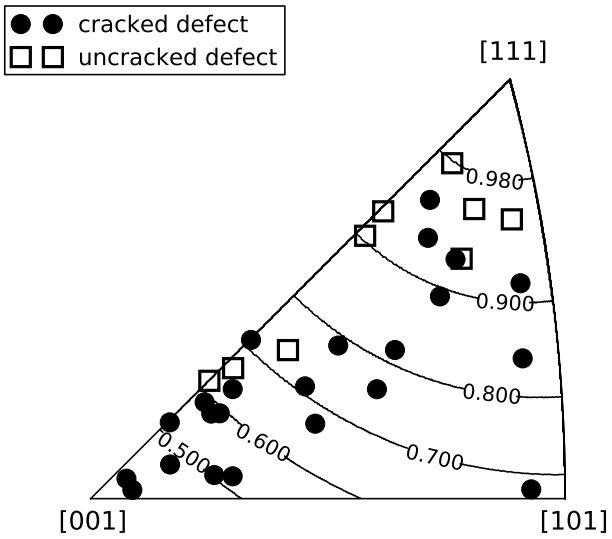

Figure 15: Orientation of the grains embedding defects, regarding the loading axis, with values of the ratio between the maximum normal stress on the slip planes and the applied uniaxial stress.

Schmid factors. The crack at the defect root (circled one) is parallel to one of the two planes of maximum Schmid factors: the crack initiation plane does not correspond to the primary slip plane (with Schmid factor of 0.48), but to the secondary slip plane (with a slightly lower Schmid factor of 0.47). This observation, although limited to one specimen among all specimens tested, is in agreement with the previous remark regarding the influence of shear stresses on fatigue crack initiation.

The present analysis, which requires the determination of Schmid factors, assumes the stress state to be uniaxial. However, while this simple approach seems sufficient for interpreting the influence of crystallographic orientation in many situations, there are some uncracked defects for which the maximum Schmid factor is significant (up to 0.47, see Figure 14). Such results could be explained

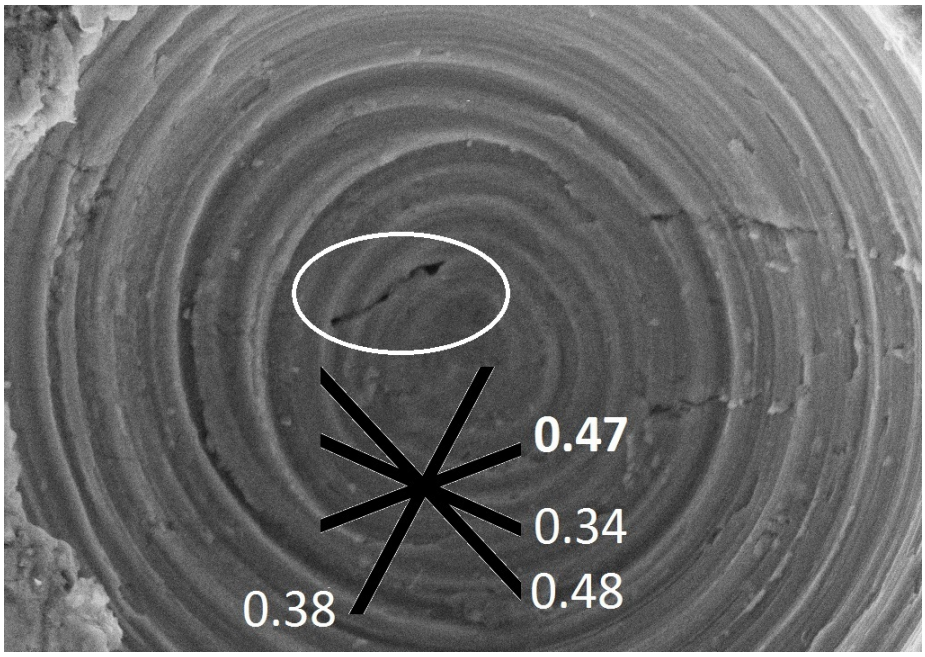

Figure 16: SEM observation of a cracked defect after cycling, from a MSD specimen, with traces of the slips planes (black lines) and values of the associated maximum Schmid factors.

by the fact that the stress field is not strictly uniaxial because of the defect and microstructural heterogeneities. Further investigations will therefore be carried out using appropriate computational methods to obtain more accurate estimations of the stress field.

5. Conclusion

In this work, the impact of geometrical defects on the HCF behavior of pure aluminium (AA1050) has been investigated. More specifically, experimental efforts have been made to better understand the role of local microstructure on fatigue crack initiation in the presence of defects. Two sizes of microstructure ($\phi_s = 100$ µm and $\phi_l = 1000$ µm) and defect ($d_s = 100$ µm and $d_l = 1000$ µm) are used.

Stress-controlled fully reversed uniaxial HCF tests have then been carried

out on specimens with defects and two grain sizes. According to fatigue test results, for a large defect, the number of cycles to obtain a 100 µm-long surface crack is higher when the grain size is reduced. However, fatigue limit, estimated as the higher stress level for which no failure occurs, is not much influenced by grain size, and the fatigue life is spent mostly in the propagation stage in all cases.

The small grain microstructure is observed to be more sensitive to the defect size. Also, when the ratio between the defect size d and the grain size ϕ is held constant, the macroscopic plastic strain amplitude associated with a 50% crack initiation probability to the defect is equivalent for both grain sizes. This suggests a strong connection between fatigue crack initiation and plasticity (as usually observed for smooth specimens) even in the presence of defect.

Finally, EBSD maps of the defect surroundings microstructure have been collected to evaluate the influence of crystallographic orientation on fatigue crack initiation. The results show that, when the defect size is small compared to the grain size, crack initiation is strongly impacted by crystallographic orientation. More specifically, crack initiation preferably occurs in crystals being favorably oriented for plastic slip. Crack initiation thus seems to be governed mostly by shear stresses, a conclusion that is consistent with the observation of an actual crack initiation plane.

To better estimate the role of microstructural heterogeneities, future work will focus on the construction of a polycrystalline plasticity model. Strain- gradient plasticity [30] will be used to introduce an internal length scale in constitutive relations. This model will provide quantitative information regarding the stress field perturbations caused by geometrical defects.

Acknowledgments

This work was financially supported by Institut Carnot ARTS and Region Pays de la Loire.

References

[1] R.S. Qi, M. Jin, X.G. Liu and B.F. Guo, Formation Mechanism of Inclusion Defects in Large Forged Pieces, J Iron Steel Res Int 23 (6), 531–538, 2016.

[2] H. Dehmani, C. Brugger, T. Palin-Luc, C. Mareau and S. Koechlin, Experimental study of the impact of punching operations on the high cycle fatigue strength of FeSi thin sheets, Int J Fatigue 82, 721–729, 2016.

[3] E. Pessard, B. Abrivard, F. Morel, F. Abroug, P. Delhaye, The effect of quenching and defects size on the HCF behaviour of Boron steel, Int J Fatigue 68, 80–89, 2014.

[4] J.O. Peters, B.L. Boyce, A.W. Thompson, R.O. Ritchie, O. Roder, Role of foreign-object damage on thresholds for high cycle fatigue in Ti-6Al-4V, Metall Mater Trans A 31 (6), 1571–1583, 2000.

[5] Y. Murakami and M. Endo, Effects of defects, inclusions and inhomogeneities on fatigue strength, Int J Fatigue 16 (3), 163–182, 1994.

[6] M. Endo and Y. Murakami, Effects of an Artificial Small Defect on Torsional Fatigue Strength of Steels, J Eng Mater Tech 109 (2), 124–129, 1987.

[7] P. Luk´as, L. Kunz, B. Weiss, R. Stickler, Notch size effect in fatigue, Fatigue Fract Eng Mater Struct 12 (3), 175–186, 1989.

[8] H.W. H¨oppel, L. May, M. Prell and M. G¨oken, Influence of grain size and precipitation state on the fatigue lives and deformation mechanisms of CP

aluminium and AA6082 in the VHCF-regime, Int J Fatigue 33 (1), 10–18, 2011.

[9] A. J¨arvenp¨a¨a, L.P. Karjalainen and M. Jaskari, Effect of grain size on fatigue behavior of Type 301LN stainless steel, Int J Fatigue 65, 93–98, 2014.

[10] G.J. Deng, S.T. Tu, X.C. Zhang, Q.Q. Wang and C.H. Qin, Grain size effect on the small fatigue crack initiation and growth mechanisms of nickel-based superalloy GH4169, Eng Fract Mech 134, 433–450, 2015.

[11] E.O. Hall, The deformation and ageing of mild steel, Proc Phys Soc London, Sec B 64 (9), 742, 1951.

[12] N.J. Petch, The cleavage strength of polycrystals, J Iron Steel Inst 174, 25–28, 1953.

[13] A. Turnbull and E.R. De Los Rios, The effect of grain size on the fatigue of commercially pure aluminium, Fatigue Fract Eng Mater Struct 18 (12), 1460–2695, 1995.

[14] K.S. Chan, Roles of microstructure in fatigue crack initiation, Int J Fatigue 32 (9), 1428–1447, 2010.

[15] J. Saga, M. Hayashi and Y. Nishio, Effect of Grain Size on Fatigue Damage in Pure Aluminium, J Soc Mater Sci Japan 26 (282), 289–295, 1977.

[16] J. Saga, M. Hayashi and Y. Nishio, Effect of Grain Size on Fatigue Crack Propagation in Aluminium, J Soc Mater Sci Japan 26 (291), 1202–1207, 1977.

[17] A.W. Thompson and W.A. Backofen, The effect of grain size on fatigue, Acta Metall 19 (7), 597–606, 1971.

[18] R. Guerchais, N. Saintier, F. Morel and C. Robert, Micromechanical investigation of the influence of defects in high cycle fatigue, Int J Fatigue 67, 159–172, 2014.

[19] C.A. Sweeney, W. Vorster, S.B. Leen, E. Sakurada, P.E. McHugh and F.P.E. Dunne, The role of elastic anisotropy, length scale and crystallographic slip in fatigue crack nucleation, J Mech Phys Solids 61 (5), 1224–1240, 2013.

[20] V.V.C. Wan, D.W. MacLachlan, F.P.E. Dunne, A stored energy criterion for fatigue crack nucleation in polycrystals, Int J Fatigue 68, 90–102, 2014.

[21] R.W. Karry and T.J. Dolan, Influence of grain size on fatigue notch- sensitivity, ASTM Proceeding (53), 789–804, 1953.

[22] P. Lorenzino and A. Navarro, Grain size effects on notch sensitivity, Int J Fatigue 70, 205–215, 2015.

[23] M. Vincent, Y. Nadot, C. Nadot-Martin and A. Dragon, Interaction between a surface defect and grain size under high cycle fatigue loading: Experimental approach for Armco iron, Int J Fatigue 87, 81–90, 2016.

[24] K.U Snowden, Dislocation arrangements during cyclic hardening and softening in A1 crystals, Acta Metall 11 (7), 675–684, 1963.

[25] Y.B. Xia, Z.G Wang and R.H. Wang, Secondary Hardening and Dislocation Evolution in Low Cycle Fatigue of Polycrystalline Aluminium, Phys Status Solidi A 120 (1), 125–132, 1990.

[26] R. Foug`eres, Early stages of fatigue damage in aluminium and aluminium alloys, J Phys IV (C7), 669–678, 1993.

[27] T. Fujii, N. Sawatari, S. Onaka and M. Kato, Cyclic deformation of pure aluminum single crystals with double-slip orientations, Mater Sci Eng A 387, 486–490, 2004.

[28] A. Giese, A. Styczynski and Y. Estrin, Cyclic hardening behaviour of polycrystalline aluminium under tension-compression, Mater Sci Eng A 124 (2), L11–L13, 1990.

[29] M. Videm and N. Ryum, Cyclic deformation and fracture of pure aluminium polycrystals, Mater Sci Eng A 219 (1), 11–20, 1996.

[30] A. Acharya, J.L. Bassani, Lattice incompatibility and a gradient theory of crystal plasticity, J Mech Phys Solids 48 (8), 1565–1595, 2000.